Contribution of radiative gluons and spin-one diquarks to the F_2 structure function

F. Zamani
Department of Physics, Villanova University, Villanova, Pennsylvania 19085, USA
(Received 28 November 2004; revised manuscript received 26 January 2006; published 22 September 2006)

We calculate unpolarized quark distribution functions and the F_2 structure functions for the proton and the neutron. The calculations are preformed in the light-cone frame. For the bare nucleon we have used three different distributions, namely, the spin-0 diquark, the spin-0 plus spin-1 diquark, and the no diquark models. By using perturbative QCD an initial gluon distribution is generated inside the core nucleon. The physical nucleon is assumed to be a superposition of the bare nucleon plus the virtual light-cone Fock states of baryon octets and decuplets and pseudoscalar meson pairs. The initial distributions are evolved. The F_2 structure functions calculated from the evolved distributions are compared with NMC and ZEUS results along with a CTEQ6M fit. Also, it is shown that the meson cloud is a contributing factor to sea-quark asymmetry and to Gottfried sum-rule violation.

DOI: 10.1103/PhysRevC.74.035204 PACS number(s): 12.39.Ki, 14.20.Dh, 14.65.Bt, 24.85.+p

I. INTRODUCTION

The original intent of this series of work was to use the meson cloud model (MCM) to gain some insight into nucleon structure [1–3]. (An extensive list of work, both experimental and theoretical, to investigate nucleon F_2 and g_1 structure functions can be found in Refs. [1–3].) We were able to show, for example, that the meson cloud is a contributing factor to sea-quark asymmetry [3], Gottfried sum-rule violation [3], rather significant strange sea-quark polarization [1,2], etc. However, there were some shortcomings; for example, the spin-0 diquark calculation of the neutron's first moment of g_1 turned out to be positive even after introduction of the gluon anomaly [1,2]. To overcome this problem we add a spin-1 diquark component to the core nucleon with the expectation that the new model will reproduce both the unpolarized and polarized structure functions reasonably well. In the present work we concentrate on the unpolarized case.

In Sec. II we briefly present a light-front representation of three-body systems and introduce the two types of wave functions that we will use for core nucleon. This will be followed by the formalism for the MCM in Sec. III. Results and discussion will be presented in Sec. IV.

II. LIGHT-FRONT REPRESENTATION OF THE NUCLEON

Since the original work by Dirac [4] several decades ago, there has been extensive use of the light-front frame to study high-energy processes. A more in-depth study of the subject for the interested reader can be found in Refs. [5–8]. Here we present basic definitions and the formalism [9,10]. A four-vector in the light-front frame is defined as

$$a = (a^+, a_-, a_\perp), \tag{1}$$

where $a^\pm = (a^\circ \pm a^3)/\sqrt{2}$ and $a_\perp = (a^1, a^2)$. Following the relativistic treatment of the nucleon by Terent'ev [11,12], we separate the center-of-mass motion of the three quarks in the nucleon from their relative motion by transforming their momenta, p_1, p_2, p_3, into total and relative momenta as follows:

$$\vec{P} = \vec{p}_1 + \vec{p}_2 + \vec{p}_3, \tag{2a}$$

$$\xi = \frac{p_1^+}{p_1^+ + p_2^+}, \quad \eta = \frac{p_1^+ + p_2^+}{P^+}, \tag{2b}$$

$$\begin{aligned} xq_\perp &= (1-\xi)p_{1\perp} - \xi p_{2\perp}, \\ Q_\perp &= (1-\eta)(p_{1\perp} + p_{2\perp}) - \eta p_{3\perp}. \end{aligned} \tag{2c}$$

Then, the Hamiltonian of the system takes the form

$$H = \frac{P_\perp^2 + \hat{M}^2}{2P^+}, \tag{3}$$

where $\hat{M}$ is the mass operator with the interaction term W:

$$\hat{M} = M + W, \tag{4a}$$

$$M^2 = \frac{Q_\perp^2}{\eta(1-\eta)} + \frac{M_3^2}{\eta} + \frac{m_3^2}{1-\eta}, \tag{4b}$$

$$M_3^2 = \frac{q_\perp^2}{\xi(1-\xi)} + \frac{m_1^2}{\xi} + \frac{m_3^2}{1-\xi}, \tag{4c}$$

with m_1, m_2, and m_3 as the constituent quarks masses. M and M_3 can be rewritten in a more transparent way in terms of the relative momenta q and Q:

$$\begin{aligned} E_1 &= \sqrt{\mathbf{q}^2 + m_1^2}, \quad E_2 = \sqrt{\mathbf{q}^2 + m_2^2}, \\ E_3 &= \sqrt{\mathbf{Q}^2 + m_3^2}, \quad E_{12} = \sqrt{\mathbf{Q}^2 + M_3^2}, \end{aligned} \tag{5a}$$

$$\xi = \frac{E_1 + q_3}{E_1 + E_2}, \quad \eta = \frac{E_{12} + Q_3}{E_{12} + E_3}, \tag{5b}$$

$$M = E_{12} + E_3, \quad M_3 = E_1 + E_2, \tag{5c}$$

where $\mathbf{q} = (q_1, q_2, q_3)$ and $\mathbf{Q} = (Q_1, Q_2, Q_3)$.

The wave function of the nucleon can be written as

$$\Psi = \Phi\chi\phi, \tag{6}$$

where Φ, χ, and ϕ are the flavor, spin, and momentum distributions, respectively. We are going to consider two different wave functions for the core nucleon. First, assume that the nucleon is a quark-diquark system. In general, the

nucleon state can be a linear combination of the spin-isospin diquark states (0,0), (0,1), (1,0), and (1,1), which can be written as

$$\begin{aligned}\Psi_1 = {} & \frac{A}{\sqrt{2}}\big[uud\big(\chi^{\rho 1}\phi_1^{\lambda 1}+\chi^{\rho 2}\phi_1^{\lambda 2}\big)-udu\big(\chi^{\rho 1}\phi_1^{\lambda 1}-\chi^{\rho 3}\phi_1^{\lambda 3}\big)\\ & -duu\big(\chi^{\rho 2}\phi_1^{\lambda 2}+\chi^{\rho 3}\phi_1^{\lambda 3}\big)\big]\\ & +\frac{B}{\sqrt{6}}\big[uud\big(\chi^{\rho 1}\phi_1^{\rho 1}+\chi^{\rho 2}\phi_1^{\rho 2}-2\chi^{\rho 3}\phi_1^{\rho 3}\big)\\ & +udu\big(\chi^{\rho 1}\phi_1^{\rho 1}-2\chi^{\rho 2}\phi_1^{\rho 2}+\chi^{\rho 3}\phi_1^{\rho 3}\big)\\ & +duu\big(-2\chi^{\rho 1}\phi_1^{\rho 1}+\chi^{\rho 2}\phi_1^{\rho 2}+\chi^{\rho 3}\phi_1^{\rho 3}\big)\big]\\ & +\frac{C}{\sqrt{2}}\big[uud\big(\chi^{\lambda 1}\phi_1^{\rho 1}+\chi^{\lambda 2}\phi_1^{\rho 2}\big)\\ & -udu\big(\chi^{\lambda 1}\phi_1^{\rho 1}-\chi^{\lambda 3}\phi_1^{\rho 3}\big)-duu\big(\chi^{\lambda 2}\phi_1^{\rho 2}+\chi^{\lambda 3}\phi_1^{\rho 3}\big)\big]\\ & +\frac{D}{\sqrt{6}}\big[uud\big(\chi^{\lambda 1}\phi_1^{\lambda 1}+\chi^{\lambda 2}\phi_1^{\lambda 2}-2\chi^{\lambda 3}\phi_1^{\lambda 3}\big)\\ & +udu\big(\chi^{\lambda 1}\phi_1^{\lambda 1}-2\chi^{\lambda 2}\phi_1^{\lambda 2}+\chi^{\lambda 3}\phi_1^{\lambda 3}\big)\\ & +duu\big(-2\chi^{\lambda 1}\phi_1^{\lambda 1}+\chi^{\lambda 2}\phi_1^{\lambda 2}+\chi^{\lambda 3}\phi_1^{\lambda 3}\big)\big]. \end{aligned} \tag{7a}$$

For the second case we assume that there is no clustering of the quarks inside the nucleon [9]:

$$\Psi_2 = \frac{-1}{\sqrt{3}}(uud\chi^{\lambda 3}+udu\chi^{\lambda 2}+duu\chi^{\lambda 1})\phi_2. \tag{7b}$$

We will be using three wave functions called Set 1, Set 2, and Set 3. Sets 1 and 2 correspond to the models that we have used in Refs. [1–3]. Set 1 is the spin-0 diquark with $A = 0.9798$, $B = -0.2$, $C = 0.0$, and $D = 0.0$ in Eq. (7a). Set 2 is Eq. (7b). Set 3 is the new model in which we choose $A = -0.7874$, $B = 0.0$, $C = 0.0$, and $D = -0.6164$ in Eq. (7a). Also, in Eq. (7), u and d represent the up and down flavor. χ^{ρ_i} and χ^{λ_i} with $i = 1, 2, 3$ represent the Melosh transformed spin wave functions [13], for example,

$$\chi_{\uparrow}^{\rho 3} = \frac{1}{\sqrt{2}}(\uparrow\downarrow\uparrow - \downarrow\uparrow\uparrow), \tag{8a}$$

$$\chi_{\downarrow}^{\rho 3} = \frac{1}{\sqrt{2}}(\uparrow\downarrow\downarrow - \downarrow\uparrow\downarrow), \tag{8b}$$

$$\chi_{\uparrow}^{\lambda 3} = \frac{1}{\sqrt{6}}(\downarrow\uparrow\uparrow + \uparrow\downarrow\uparrow - 2\uparrow\uparrow\downarrow), \tag{8c}$$

$$\chi_{\downarrow}^{\lambda 3} = \frac{1}{\sqrt{6}}(2\downarrow\downarrow\uparrow - \downarrow\uparrow\downarrow - \uparrow\downarrow\downarrow). \tag{8d}$$

The spin wave function of the ith quark is

$$\uparrow = R_i\begin{pmatrix}1\\0\end{pmatrix}, \quad \downarrow = R_i\begin{pmatrix}0\\1\end{pmatrix}. \tag{9}$$

In Eq. (9), R_i are the Melosh matrices:

$$R_1 = \frac{1}{\sqrt{a^2+Q_\perp^2}\sqrt{c^2+q_\perp^2}} \times \begin{pmatrix} ac - q_R Q_L & -aq_L - cQ_L \\ cQ_R + aq_R & ac - q_L Q_R \end{pmatrix}, \tag{10a}$$

$$R_2 = \frac{1}{\sqrt{a^2+Q_\perp^2}\sqrt{d^2+q_\perp^2}} \times \begin{pmatrix} ad + q_R Q_L & -aq_L - dQ_L \\ dQ_R - aq_R & ad - q_L Q_R \end{pmatrix}, \tag{10b}$$

$$R_3 = \frac{1}{\sqrt{b^2+Q_\perp^2}}\begin{pmatrix} b & Q_L \\ -Q_R & b \end{pmatrix}, \tag{10c}$$

where

$$a = M_3 + \eta M, \quad b = m_3 + (1-\eta)M, \tag{11a}$$

$$c = m_1 + \xi M_3, \quad d = m_2 + (1-\xi)M_3, \tag{11b}$$

$$q_R = q_1 + iq_2, \quad q_L = q_1 - iq_2, \tag{11c}$$

$$Q_R = Q_1 + iQ_2, \quad Q_L = Q_1 - iQ_2. \tag{11d}$$

The functions $\phi_1^{\rho i}$, and $\phi_1^{\lambda i}$, with $i = 1, 2, 3$, and ϕ_2 are the momentum wave functions, which we take to be of the following form:

$$\phi_1^{\rho i} = N_{\rho i}(X_j - X_k)\phi_1^{si}/X_T, \tag{12a}$$

$$\phi_1^{\lambda i} = N_{\lambda i}(X_j + X_k - 2X_i)\phi_1^{si}/X_T, \tag{12b}$$

with $i \neq j \neq k$, and [9]

$$\phi_2 = \frac{N}{(M^2+\beta^2)^{3.5}}. \tag{12c}$$

Also,

$$\begin{aligned} X_3 = {} & \frac{Q_\perp^2}{2\eta(1-\eta)\beta_Q^2} + \frac{q_\perp^2}{2\eta\xi(1-\xi)\beta_q^2} + \frac{m_1^2}{2\eta\xi\beta_q^2} \\ & + \frac{m_2^2}{2\eta(1-\xi)\beta_q^2} + \frac{m_3^2}{2(1-\eta)\beta_Q^2}, \end{aligned} \tag{13a}$$

$$\begin{aligned} X_2 = {} & q_\perp^2 \frac{(1-\eta)(1-\xi)\beta_Q^2 + \xi\beta_q^2}{2\beta_Q^2\beta_q^2\eta\xi(1-\xi)(1-\eta+\xi\eta)} \\ & + Q_\perp^2 \frac{(1-\xi)(1-\eta)\beta_q^2 + \xi\beta_Q^2}{2\beta_Q^2\beta_q^2\eta(1-\eta)(1-\eta+\xi\eta)} \\ & + q_\perp Q_\perp \frac{\beta_Q^2 - \beta_q^2}{\beta_Q^2\beta_q^2\eta(1-\eta+\xi\eta)} + \frac{m_1^2}{2\eta\xi\beta_q^2} \\ & + \frac{m_2^2}{2\eta(1-\xi)\beta_Q^2} + \frac{m_3^2}{2(1-\eta)\beta_q^2}, \end{aligned} \tag{13b}$$

$$\begin{aligned} X_1 = {} & q_\perp^2 \frac{(1-\xi)\beta_q^2 + \xi(1-\eta)\beta_Q^2}{2\beta_Q^2\beta_q^2\eta\xi(1-\xi)(1-\xi\eta)} \\ & + Q_\perp^2 \frac{(1-\xi)\beta_Q^2 + \xi(1-\eta)\beta_q^2}{2\beta_Q^2\beta_q^2\eta(1-\xi)(1-\xi\eta)} \\ & - q_\perp Q_\perp \frac{\beta_Q^2 - \beta_q^2}{\beta_Q^2\beta_q^2\eta(1-\xi\eta)} + \frac{m_1^2}{2\eta\xi\beta_Q^2} \\ & + \frac{m_2^2}{2\eta(1-\xi)\beta_q^2} + \frac{m_3^2}{2(1-\eta)\beta_q^2}, \end{aligned} \tag{13c}$$

$$X_T = X_1 + X_2 + X_3, \tag{13d}$$

and

$$\phi_1^{\rm si} = \frac{1}{(1+X_T)^{\rm ni}}. \tag{13e}$$

In these equations β_Q, β_q, and β are confinement scale parameters and N_{ρ_i}, N_{λ_i}, and N are normalization constants.

III. THE MESON CLOUD MODEL IN THE LIGHT-CONE FRAME

Using the convolution model, one can decompose the physical nucleon in terms of the core nucleon and intermediate, virtual meson-baryon states [1–3 and references therein]:

$$|N\rangle = Z^{1/2}\left[|N\rangle_{\rm bare} + \sum_{BM}\beta_{BM}|BM\rangle\right], \tag{14}$$

where Z is the probability of the physical nucleon being in the core state, BM stands for a virtual baryon-meson state, and β_{BM} is the probability amplitude for the physical nucleon being in the BM state. The summation in Eq. (14), in general, includes all physically possible pairs from the meson octet and baryon octet and decuplet. In terms of the quark distributions one can write

$$q_N(x) = Z\left\{q_{N,\rm core}(x) + \sum_{MB}\alpha_{MB}\left[\int_x^1 n_{MB}(y)q_M\left(\frac{x}{y}\right)\frac{dy}{y} + \int_x^1 n_{BM}(y)q_B\left(\frac{x}{y}\right)\frac{dy}{y}\right]\right\}, \tag{15}$$

where x is the fraction of the total momentum of the nucleon being carried by quark q, α_{MB} are spin-flavor Clebsch-Gordan coefficients, n_{MB} and n_{BM},the splitting functions, are the probabilities of the nucleon being in state MB or BM, respectively, and y is the fraction of the momentum being carried by the meson (baryon) in $n_{MB}(y)$ ($n_{BM}(y)$). The splitting functions must satisfy the following equations:

$$n_{MB}(y) = n_{BM}(1-y) \tag{16}$$

and

$$\langle x n_{MB}\rangle + \langle x n_{BM}\rangle = \langle n_{BM}\rangle. \tag{17}$$

In Eq. (17) $\langle n\rangle$ and $\langle xn\rangle$ are the first and second moments of the splitting functions. Equation (16) ensures the global charge conservation and Eq. (17) ensures ensures momentum conservation.

To calculate $q_N(x)$ one needs to know $q_{N,\rm core}(x)$, $q_M(x)$, $q_B(x)$, and $n_{MB}(x)$ explicitly. To calculate the core quark distribution we use the following expression [14]:

$$q_{i,\rm core}(x) = \int [dx][dk_\perp]\delta(x_i - x)|\phi(x_i, k\perp i)|^2, \tag{18}$$

with

$$[dx] = \frac{dx1\,dx2\,dx3}{\sqrt{(x_1x_2x_3)}}, \qquad [dk_\perp] = dk_{\perp 1}dk_{\perp 2}, \qquad \sum_i x_i = 1, \qquad \sum_i k_{\perp i} = 0, \tag{19}$$

where $x_1 = \xi\eta$, $x_2 = \eta(1-\xi)$, and $x_3 = 1-\eta$. For ϕ in this equation we use the expression in Eq. (12). We calculate $q_M(x)$ in the following way [15]:

$$q_M(x) = \frac{1}{4}\int \frac{dk_\perp}{x(1-x)} M_\circ(x,k_\perp)|\Phi_\pi(x,k_\perp)|^2, \tag{20a}$$

where

$$M_\circ^2(x,k_\perp) = \frac{k_\perp^2 + m_q^2}{x(1-x)}, \tag{20b}$$

$$\Phi_\pi(x,k_\perp) = Ne^{\frac{-k^2}{(2\Lambda_\pi)^2}}, \tag{20c}$$

and

$$k^2 = \left(k_\perp^2/4 + (x-1/2)^2 m_q^2\right)/x(1-x), \tag{20d}$$

$q_B(x)$ is calculated using the core distributions. To calculate $n_{MB}(x)$ we use [16,17]

$$n_{MB}(x) = \frac{g_{NMB}^2}{16\pi^2}\int_0^1 \frac{dy}{y(1-y)}\int_0^\infty dk_\perp^2 \frac{\left|\Gamma_{MB}\left(M_{MB}^2\right)\right|^2}{\left(M_{MB}^2 - m_N^2\right)^2}\frac{1}{y} \times [(m_B - ym_N)^2 + \mathbf{k}_\perp^2] \tag{21a}$$

for meson-baryon octet intermediate states and

$$n_{MB}(x) = \frac{g_{NMB}^2}{16\pi^2}\int_0^1 \frac{dy}{y(1-y)}\int_0^\infty dk_\perp^2 \frac{\left|\Gamma_{MB}\left(M_{MB}^2 0\right)\right|^2}{\left(M_{MB}^2 - m_N^2\right)^2} \times \frac{1}{6m_B^2 y^3}\left[(m_B + ym_N)^2 + \mathbf{k}_\perp^2\right]^2 \times [(m_B - ym_N)^2 + \mathbf{k}_\perp^2] \tag{21b}$$

for meson-baryon decuplet intermediate states. In Eqs. (20) and (21), $\Gamma(M_{MB}^2)$ is the vertex form factor, which is parameterized by the exponential function of the invariant mass M_{MB} of the intermediate baryon-meson state:

$$\Gamma\left(M_{MB}^2\right) = e^{-\frac{\left(M_{MB}^2 - m_N^2\right)}{\Lambda_{MB}^2}}, \tag{22}$$

with Λ_{MB} free parameters that are determined by fitting experimental data. Putting all these pieces together and using all possible intermediate baryon-meson states one could calculate the physical quark distributions in the proton and the neutron. In the current work we use pseudoscalar mesons and baryon octet and decuplet intermediate states. These initial distributions are calculated at some initial low $Q_\circ^2$. To be able to compare our results with experiments, we evolve these initial distributions using DGLAP equations [18–20] to some final high Q^2. The DGLAP equations are

$$\frac{dq^i(x,t)}{dt} = \frac{\alpha(t)}{2\pi}\int_x^1 \frac{dy}{y}\left[\sum_{j=1}^{2f} q^j(y,t)P_{q^iq^j}\left(\frac{x}{y}\right) + G(y,t)P_{q^iG}\left(\frac{x}{y}\right)\right], \tag{23a}$$

$$\frac{dG(x,t)}{dt} = \frac{\alpha(t)}{2\pi}\int_x^1 \frac{dy}{y}\left[\sum_{j=1}^{2f} q^j(y,t)P_{Gq^j}\left(\frac{x}{y}\right) + G(y,t)P_{\rm GG}\left(\frac{x}{y}\right)\right] \tag{23b}$$

TABLE I. Parameters used in Sets 1, 2, and 3. Here m_u, m_d, β_Q, and β_q are all in GeV, and μ_p and μ_n are in nuclear magneton units. Sets 1 and 3 represent our diquark-quark models, whereas Set 2 represents parameters used by Schlumpf [9,10].

	m_u	m_d	β_Q	β_q	n_1	n_2	n_3	μ_p	μ_n
Set 1	0.250	0.210	0.25	0.45	2.8	2.8	2.6	2.82	−1.61
Set 2	0.263	0.263	0.607	0.607	3.5	3.5	3.5	2.81	−1.66
Set 3	0.250	0.210	0.25	0.45	2.8	2.8	2.6	2.79	−1.68

for singlet distributions and

$$\frac{dq^{\mathrm{NS}}(x,t)}{dt} = \frac{\alpha(t)}{2\pi}\int_x^1 \frac{dy}{y} q^{\mathrm{NS}}(y,t) P^{\mathrm{NS}}\left(\frac{x}{y}\right) \tag{23c}$$

for nonsinglet distributions. In Eq. (23) α is the QCD running coupling constant, q and G are the quark and gluon distribution functions, respectively, the Ps are the splitting functions, f is the number of flavors, and t is defined as

$$t = \ln\left(Q^2/Q_\circ^2\right). \tag{23d}$$

Having the distribution functions one can calculate the nucleon structure functions:

$$2F_1 = F_2/x = \sum_i^f e_i^2 [q^i(x) + \bar{q}^i(x)], \tag{24}$$

where e_i is the charge of the ith quark.

IV. RESULTS AND DISCUSSION

In Table I we present the parameters, in energy units of GeV, that have been used in Eqs. (12), (13), (16), and (17) to calculate the quark distribution functions and the proton and neutron structure functions. Set 1 represents the spin-0 diquark distribution for the core nucleon. Set 2 is the set of parameters used by Schlumpf [9] and represents a symmetrical distribution of quarks inside the nucleon. Set 3 is a superposition of the spin-0 and spin-1 diquark wave functions. In our calculations we have used three other sets identified as Set 1g, Set 2g, and Set 3g. These sets are identical to Set 1, Set 2, and Set 3 in all respects but have gluons present in the initial distributions before the introduction of the meson cloud. We use the work by Barone and collaborators [21] to build up a gluon distribution inside the nucleon. (More details are presented in the Appendix.) In this approach one starts with the bare nucleon and builds the gluon distribution in small increments of Q^2 (see the Appendix). In Fig. 1 we show the gradual change in the Set-3 u-quark distribution from bare nucleon to the final state of $Q^2 = 0.5$ GeV^2. The total number of gluons at this stage turns out to be about 6 and they carry around 27% of the nucleon's momentum.

For the cutoff parameters we have used a universal value of 0.880 GeV for all vertices. This numerical value is well within the acceptable range [3]. For the coupling constants we choose

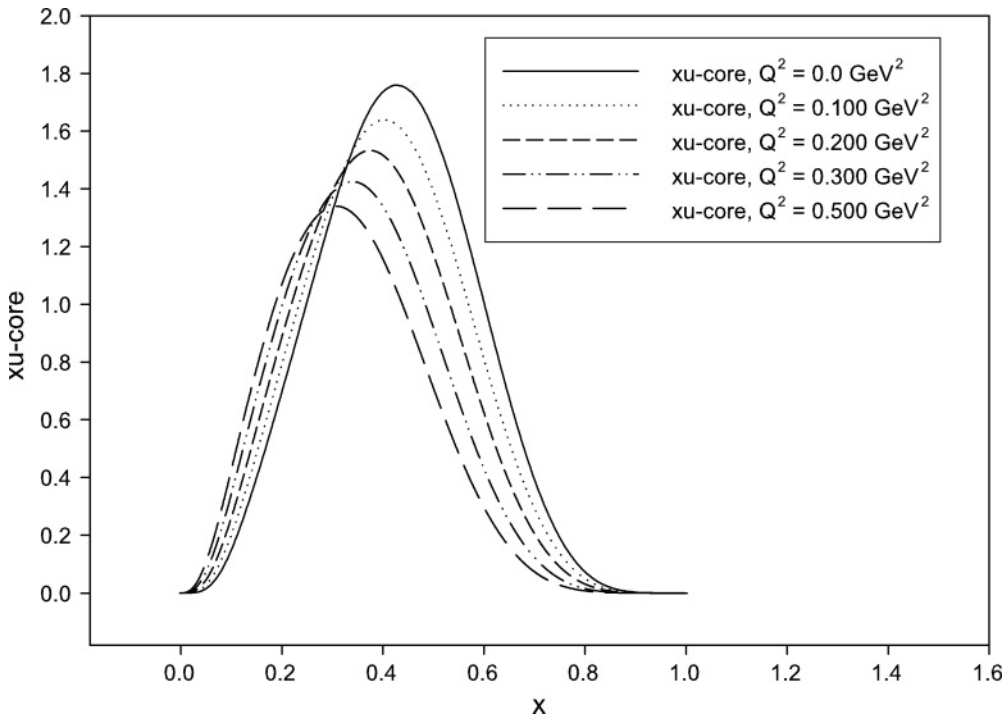

FIG. 1. xu-core distributions for Set 3 at different Q^2 values, as gluons are built up inside the nucleon.

TABLE II. Initial momentum transferred squared and QCD scale parameter for this work, NMC [26,27], ZEUS [28,29], CTEQ6M four-flavor, and CTEQ6M five-flavor [31].

	This work	NMC	ZEUS	CTEQ6M-4f	CTEQ6M-5f
$Q_0^2(\mathrm{GeV}^2)$	0.50	20.0	7.0	1.69	1.69
$\Lambda(\mathrm{GeV})$	0.318	0.250	0.255	0.326	0.226

[16–22] $g^2_{p\pi^\circ p}/4\pi = 13.6$ and $g^2_{p\Delta^{++}\pi^-}/4\pi = 10.85\ \mathrm{GeV}^{-2}$. Other coupling constants are related to these two through the quark model [22–24].

Starting at the initial momentum transferred the quark distributions are evolved by using the code by Miyama and Kumano [25] to the final momentum transferred and compared with NMC [26,27] and ZEUS [28–30] results and a CTEQ6M fit [31]. The code uses the $\bar{M}S$ renormalization scheme and calculates Q^2 evolution to the next-to-leading order of running coupling constant using brute-force numerical integration. Some of the input parameters are the initial and final momentum transferred squared, the QCD scale parameter, and the number of flavors, which can be three or four. Table II presents the initial momentum transferred squared and the QCD scale parameter for our work, NMC, ZEUS, and CTEQ6M. The NMC data are reproduced using Eq. (2) in Ref. [27]. The ZEUS data are reproduced using the ZEUS-S QCD NLO fit [28,29]. To generate CTEQ6M results we have used their Λ_{5f} [31], where $5f$ means five flavors. However, our value is more in line with Λ_{4f}, as is shown in Table II. All initial distributions are evolved to the final momentum transferred of 70 GeV^2. In Figs. 2 and 3 we present our initial xu-valence and xd-valence quark distributions for the three models and compare them with the corresponding CTEQ6M distributions [31]. A few points are to be made here. One is that the introduction of the gluons improves the distributions considerably. This is evident by observing the differences between Set-3 and Set-3g distributions. Another point is that the addition of spin-1 leads to a slight reduction in the difference between our model and the CTEQ6M in the midregion of x values. Also, the Set-2g u-valence distribution is lower than the diquark models from $x \geqslant 0.3$ to $x \sim 0.7$. The same is true, to a lesser degree, for d-valence distributions in the range $x \geqslant 0.2$ to $x \sim 0.5$. This is the reason that the structure function calculated using Set 2 undershoots the observation for the aforementioned range of x to a higher degree and therefore it is not a suitable model for the unpolarized case. In Fig. 4 we present sea-quark asymmetry generated by pseudoscalar mesons and their corresponding baryons. Our results show that the meson cloud does indeed play a role as a source of sea-quark asymmetry. However, the CTEQ6M data peak at much lower x. The addition of a vector meson to the cloud could reduce the difference in magnitude of our results from those of CTEQ6M but we do not expect much shift in the position of the peak. One point has to be made is that, in the CETQ6M fit, the strange quark distribution is assumed to be the same as the antistrange quark distribution. However, in reality we know that that is not the case and our results do indeed show the strange quark asymmetry. Of course, the net strangeness inside the nucleon is zero and in our case $\int_0^1 [s(x) - \bar{s}(x)]dx \sim 10^{-04} \sim 0$. We evolve the initial distributions to $Q_f^2 = 70\ \mathrm{GeV}^2$. Having seen the significant difference between the initial Set-3 and Set-3g distributions,

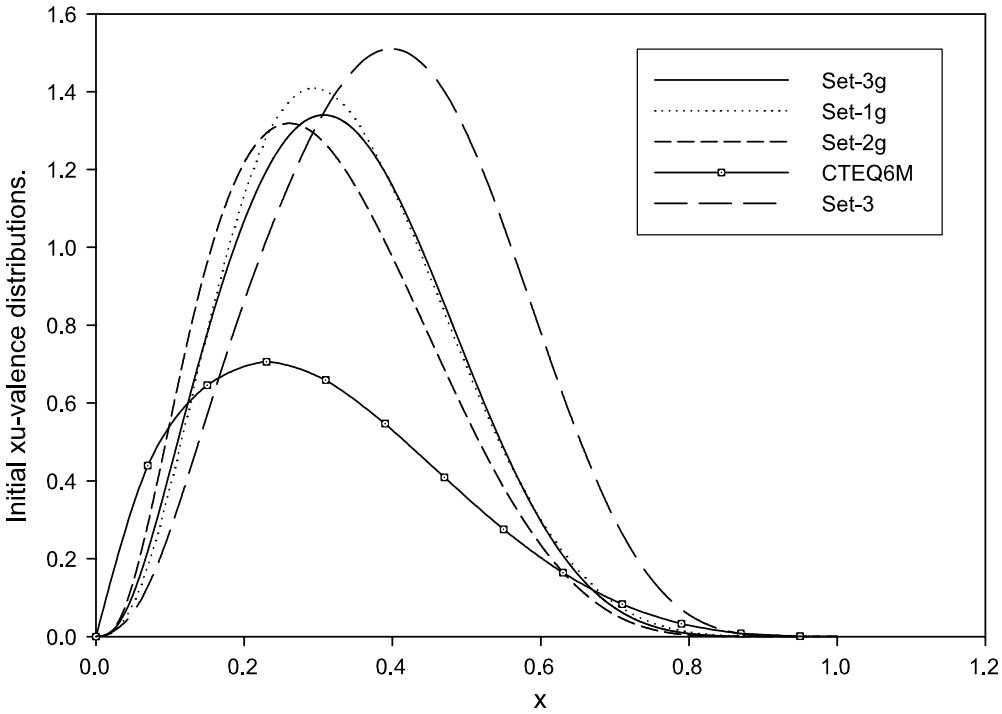

FIG. 2. Initial xu-valence distributions for Set 3g (spin-0 and spin-1 diquark), Set 1g (only spin-0 diquark), Set 2g (no diquark), Set 3, and CTEQ6M.

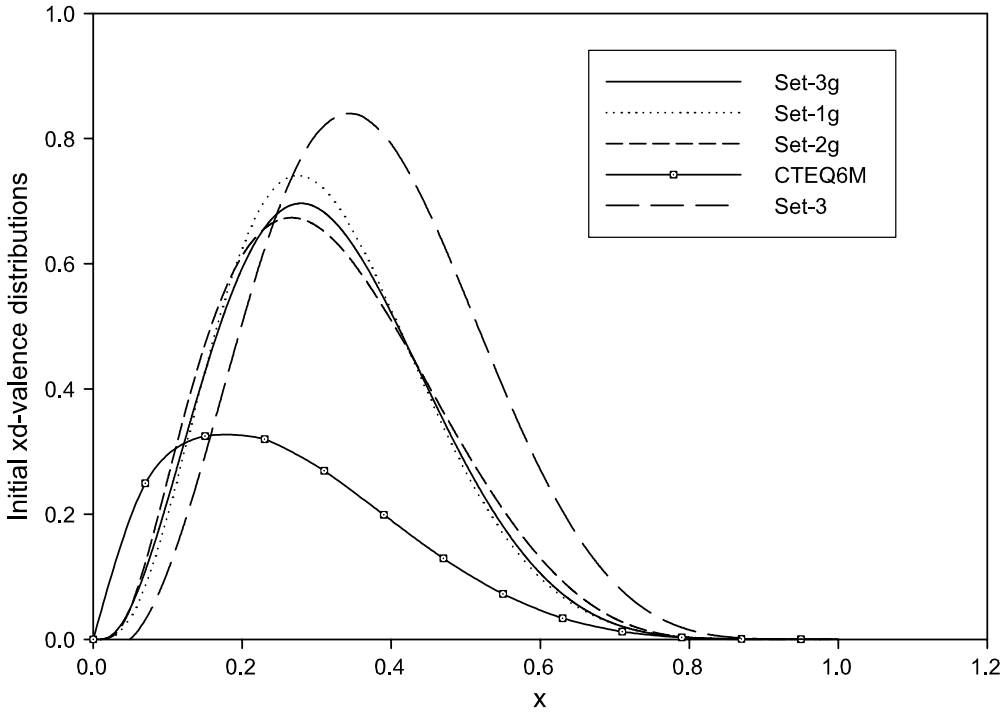

FIG. 3. Initial xd-valence distributions for Set 3g (spin-0 and spin-1 diquark), Set 1g (only spin-0 diquark), Set 2g (no diquark), Set 3, and CTEQ6M.

we will consider Set 3gs and not Set 3. The results for xu-valence and xd-valence distributions are shown in Figs. 5 and 6. As expected there is a shift to lower x for the distributions. Also, the differences between our models and CTEQ6M and ZEUS have reduced noticeably. For $x \geqslant 0.5$ there is rather good agreement between both diquark models and the ZEUS result. Figures 7 and 8 compare the sea-quark and gluon distributions of our models with ZEUS and CTEQ6M. For both cases our model results are somewhat lower than those of CTEQ6M and ZEUS for $x \geqslant 0.05$; sea-quark Set 3g is

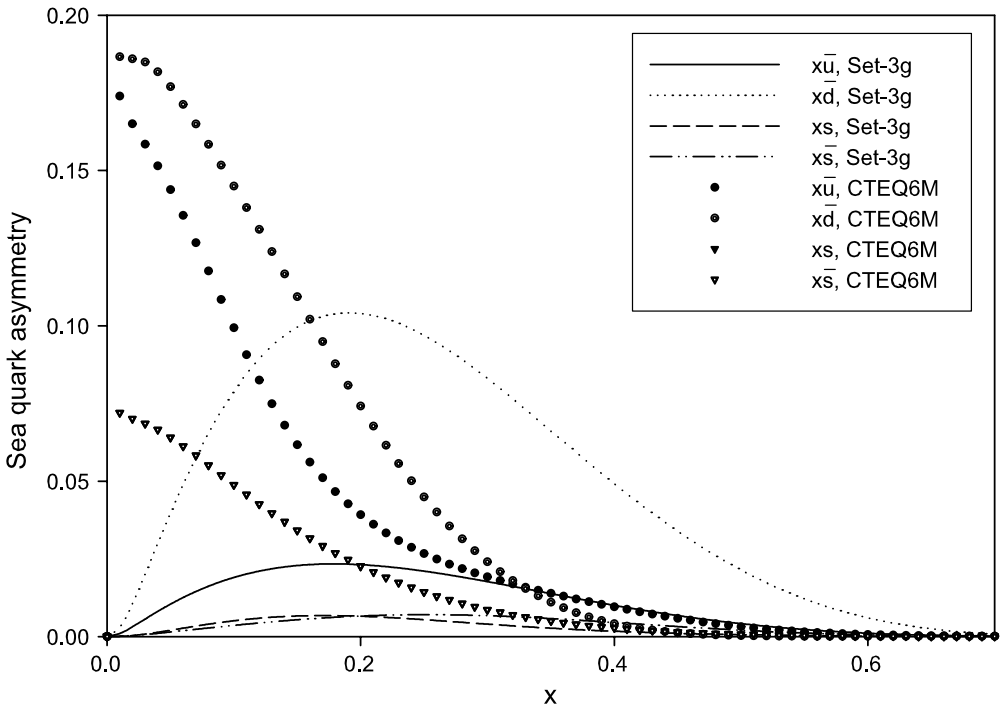

FIG. 4. Sea-quark asymmetry owing to the meson cloud for Set 3g (spin-0 and spin-1 diquark) and CTEQ6M.

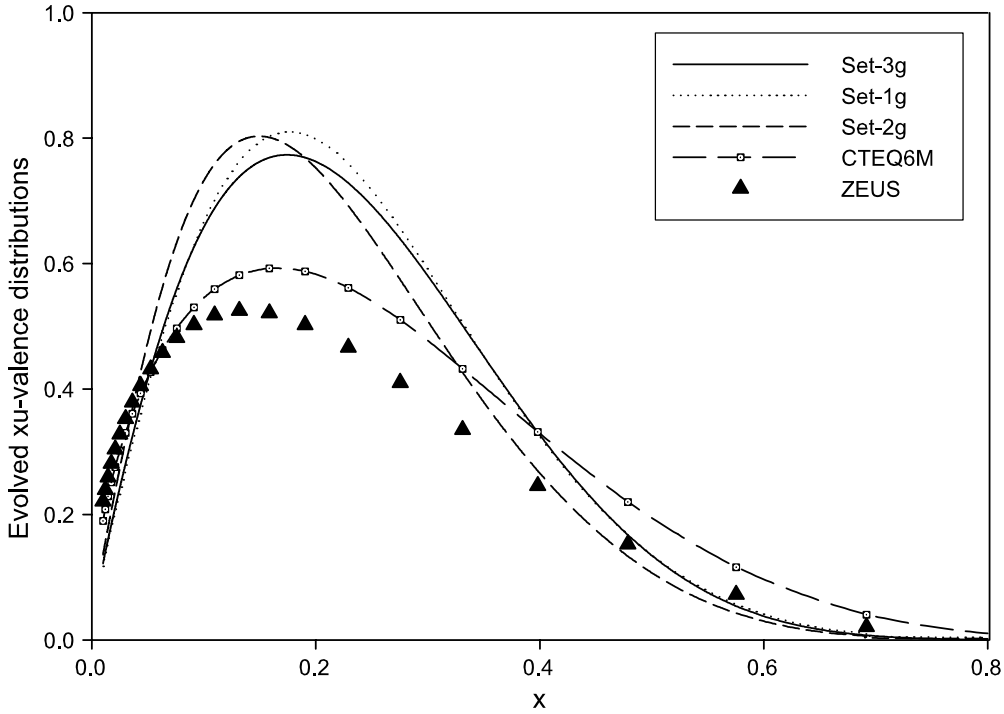

FIG. 5. Evolved xu-valence distributions for Set 3g (spin-0 and spin-1 diquark), Set 1g (only spin-0 diquark), Set 2g (no diquark), CTEQ6M, and ZEUS.

closest to CTEQ6M and ZEUS, whereas Set 2g has the largest difference. The addition of vector mesons to the cloud will most likely improve our results. For $x \leqslant 0.02$ all three models overshoot observation.

We use the final quark distributions to calculate the F_2 structure functions for the proton and the neutron. Figures 9 and 10 show the structure function F_2 for the proton and the neutron, respectively. In both cases the three

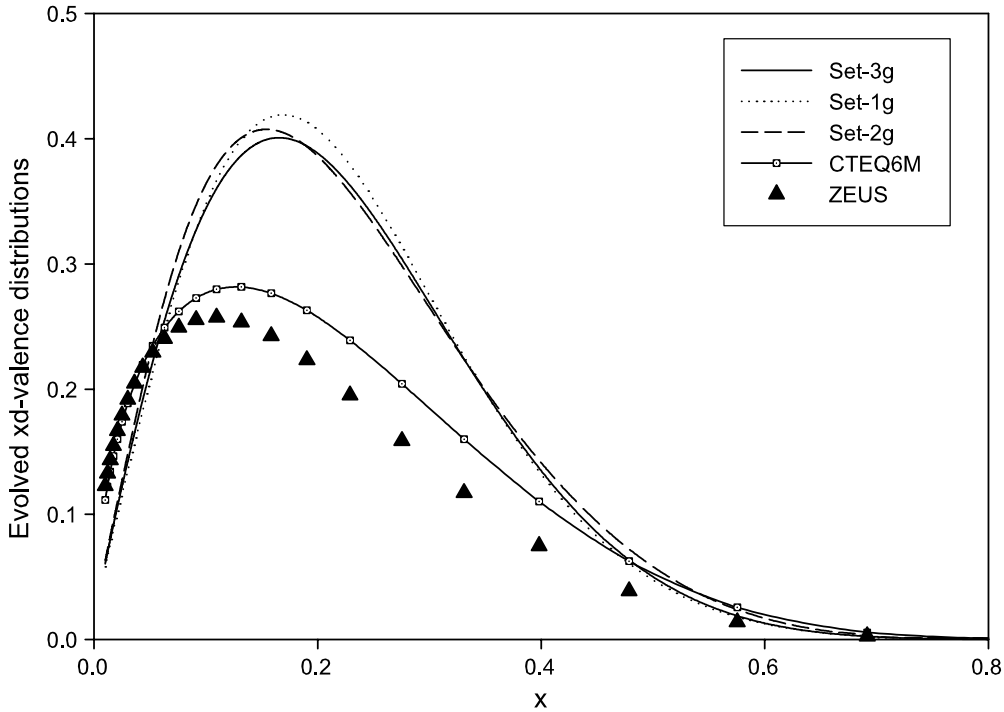

FIG. 6. Evolved xd-valence distributions for Set 3g (spin-0 and spin-1 diquark), Set 1g (only spin-0 diquark), Set 2g (no diquark), CTEQ6M, and ZEUS.

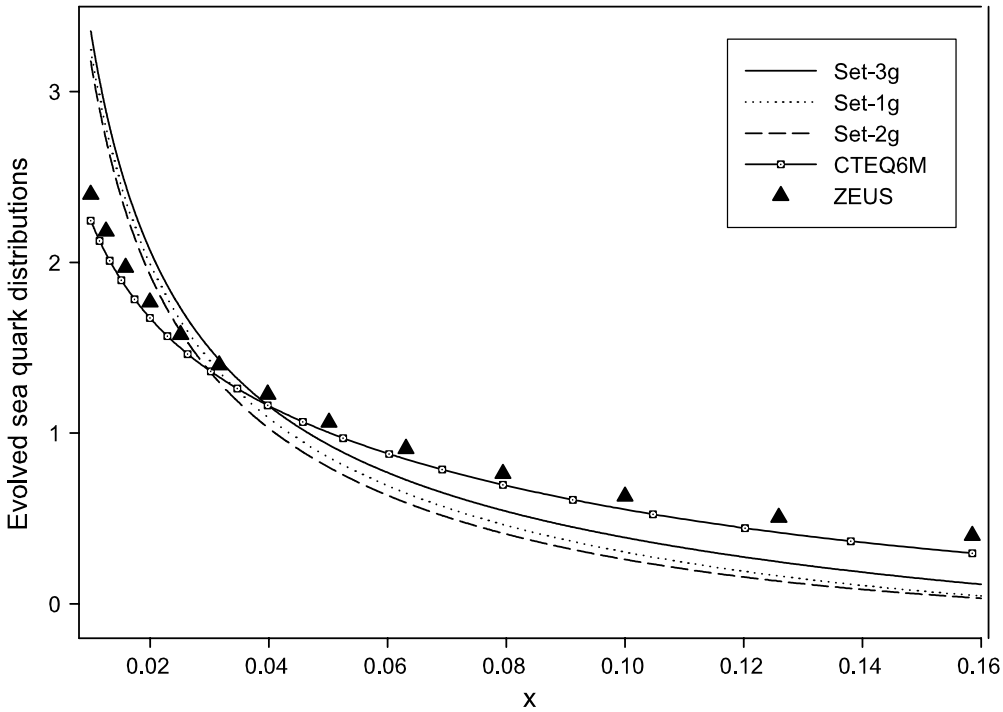

FIG. 7. Evolved sea-quark distributions for Set 3g (spin-0 and spin-1 diquark), Set 1g (only spin-0 diquark), Set 2g (no diquark), CTEQ6M, and ZEUS.

models are within the ZEUS error-bar range all the way down to $x \sim 0.02$. Between $x = 0.02$ and $x = 0.1$ our F_{2p} has a better agreement with data compared with F_{2n}. For $x > 0.1$ the situation is reversed. For $x < 0.02$, our results diverge from data rather significantly, indicating that the model is not suitable for that range. Figures 11 and 12 show $F_{2p} - F_{2n}$ and F_{2n}/F_{2p}, respectively. These two graphs demonstrate clearly that the diquark models are indeed in better agreement

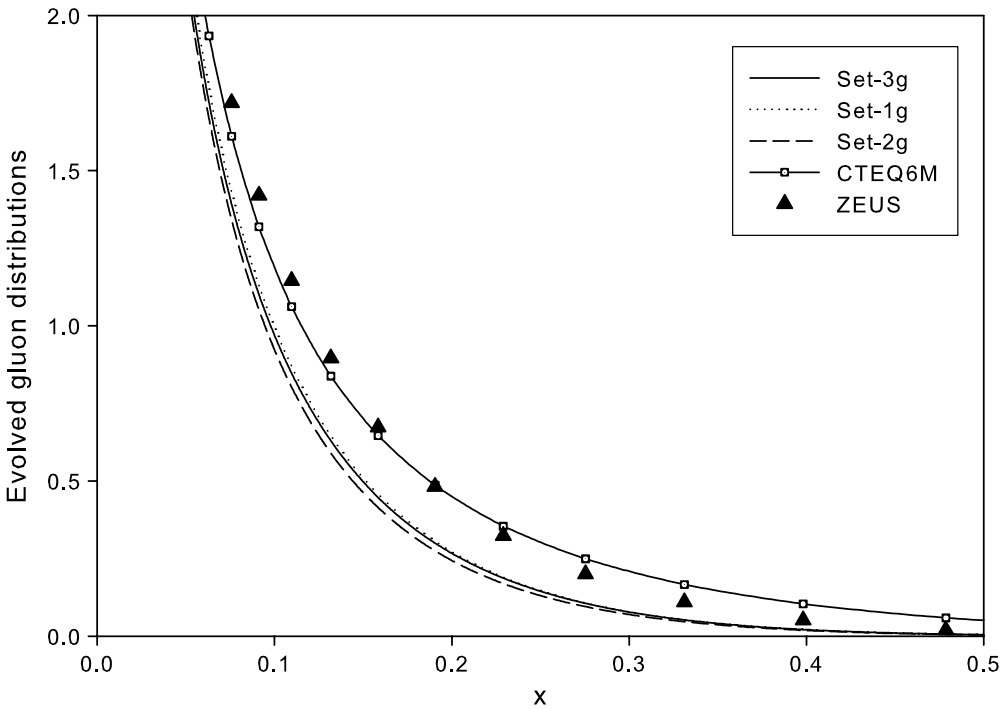

FIG. 8. Evolved gluon distributions for Set 3g (spin-0 and spin-1 diquark), Set 1g (only spin-0 diquark), Set 2g (no diquark), CTEQ6M, and ZEUS.

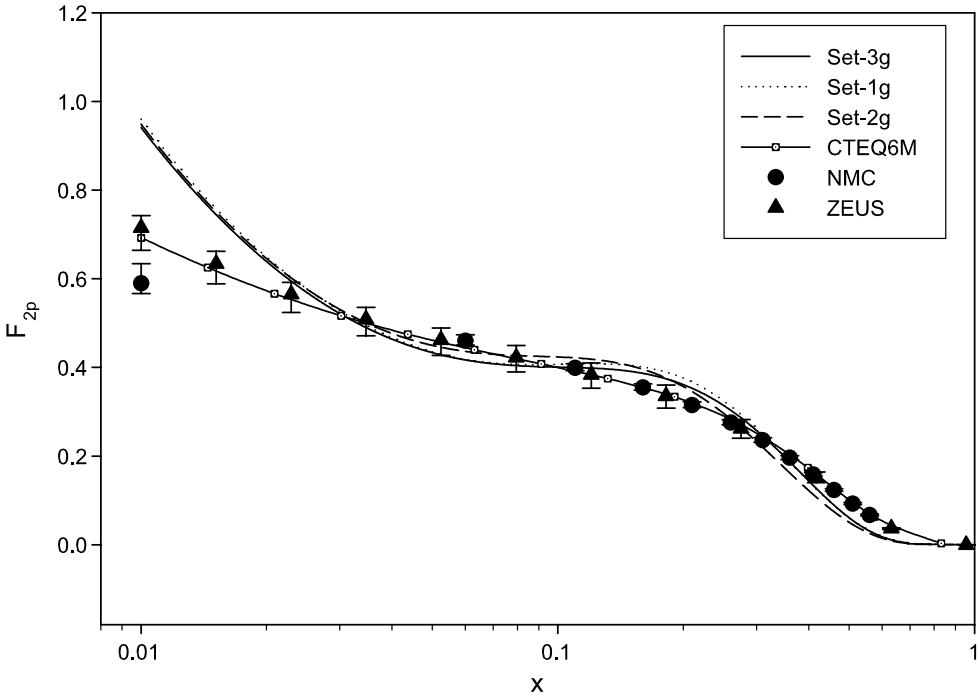

FIG. 9. F_2 structure function for the proton. Circles and triangles are NMC and ZEUS fits, respectively, at $Q^2 = 70$ GeV^2. The line-symbol is the CTEQ6M fit. The lines are the results of our model Set 3g (spin-0 and spin-1 diquark), Set 1g (only spin-0 diquark), Set 2g (no diquark), and Set 3.

with observation than the case in which there is no diquark.

In the quark model, the Gottfried sum rule (GSR) [32] can be written as

$$\int_0^1 \frac{dx}{x}[F_{2p}(x, Q^2) - F_{2n}(x, Q^2)] = \frac{1}{3}. \qquad (25)$$

NMC [33,34] results show deviations from the right-hand side of Eq. (25):

$$\int_0^1 \frac{dx}{x}[F_{2p}(x, 4\ \text{GeV}^2) - F_{2n}(x, 4\ \text{GeV}^2)] = 0.240 \pm 0.034 \pm 0.021. \qquad (26)$$

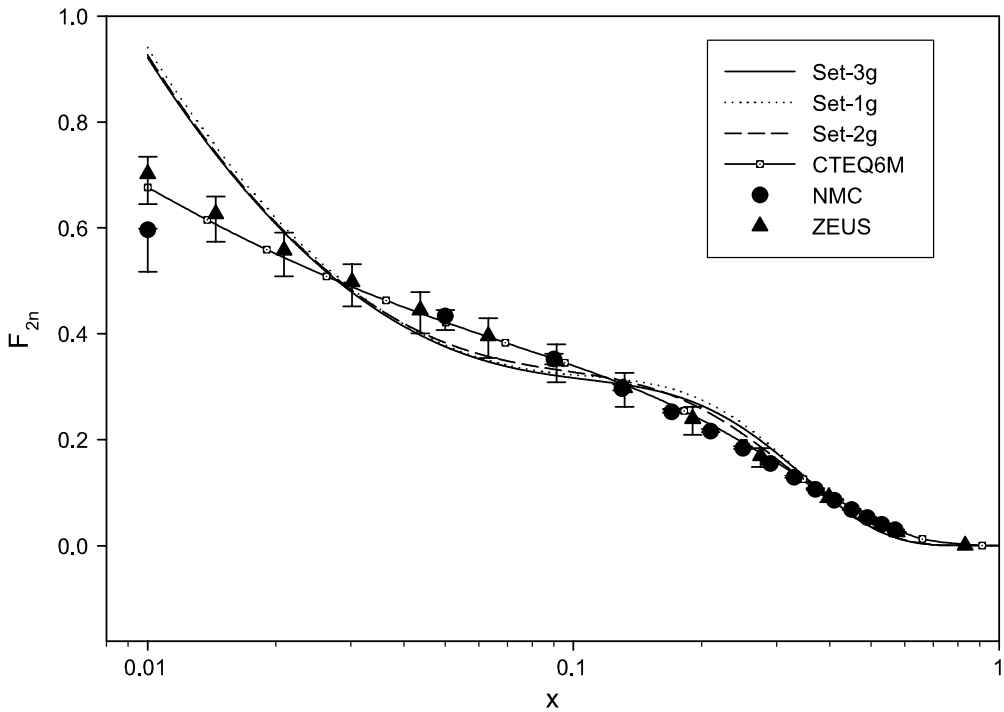

FIG. 10. F_2 structure function for the neutron. Circles and triangles are NMC and ZEUS fits, respectively, at $Q^2 = 70$ GeV^2. The line symbol is the CTEQ6M fit. The lines are the results of our model Set 3g (spin-0 and spin-1 diquark), Set 1g (only spin-0 diquark), Set 2g (no diquark), and Set 3.

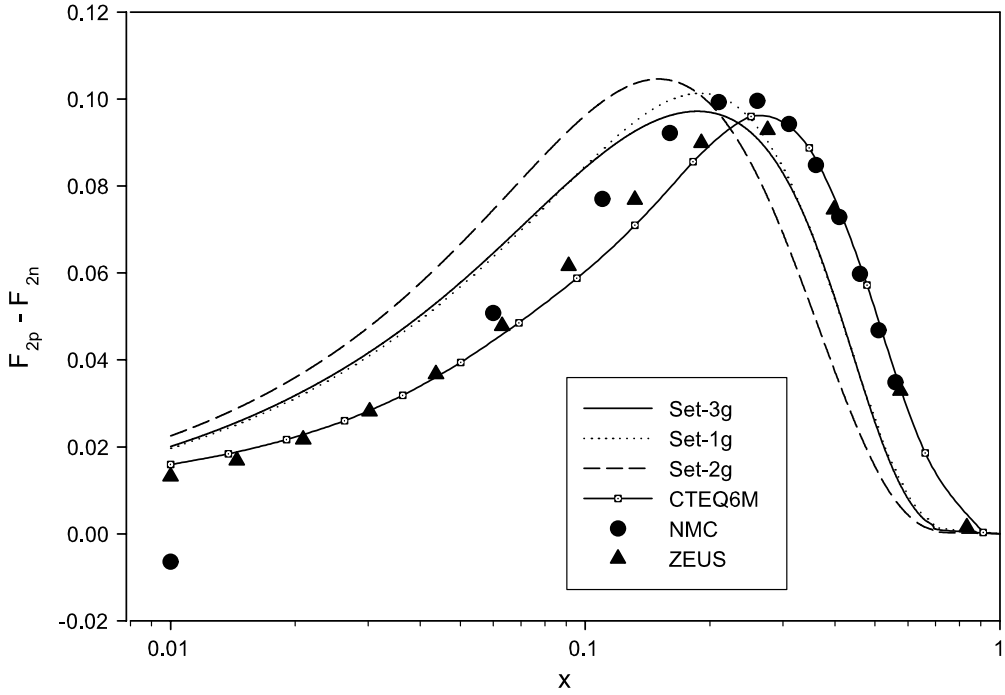

FIG. 11. Difference in proton and neutron F_2 structure functions. Circles and triangles are NMC and ZEUS fits, respectively, at $Q^2 = 70$ GeV^2. The line symbol is the CTEQ6M fit. The lines are the results of our model Set 3g (spin-0 and spin-1 diquark), Set 1g (only spin-0 diquark), Set 2g (no diquark), and Set 3.

This deviation can be attributed to the flavor asymmetry of the nucleon sea. In Table III, we present GSR results for our models, NMC, ZEUS, and CTEQ6M at $Q^2 = 70$ GeV^2. For NMC and ZEUS calculations we have used their parametrizations and integrated over x from zero to one. Therefore, one can conclude that the MCM does indeed contribute to the GSR. However, the pseudoscalar meson cloud alone is not enough to reproduce the observation. However, the two diquark model predications are closer to the observation relative to the symmetrical case.

Now we briefly summarize our work. We used a quark-diquark model for the bare nucleon. We considered two different diquark distributions: one only spin 0 and the other a superposition of spin 0 and spin 1. Both models agreed

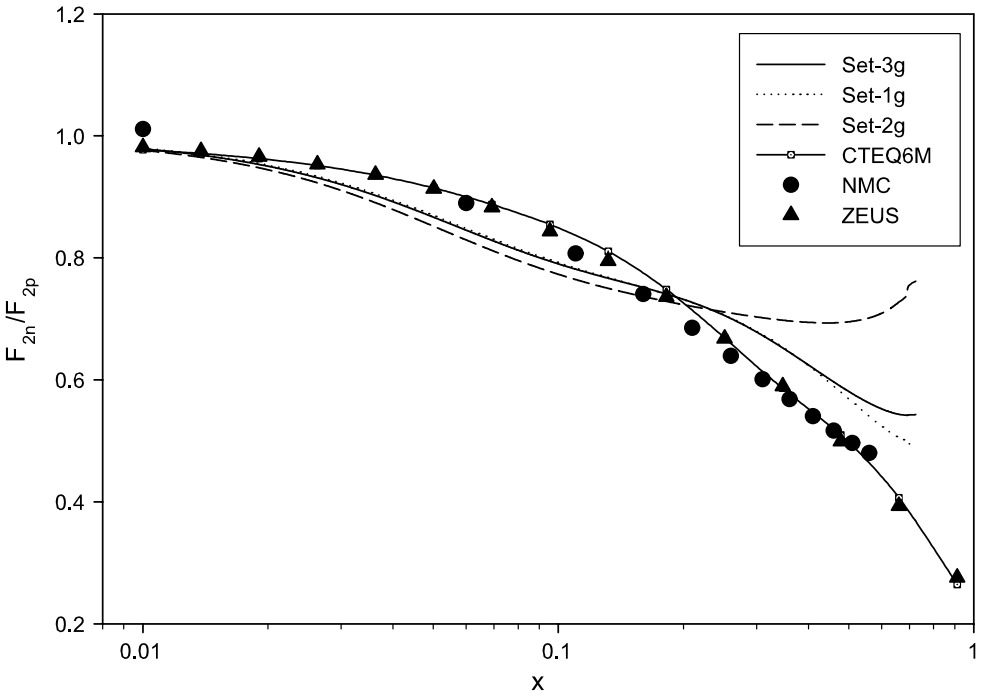

FIG. 12. Ratio of the neutron to proton F_2 structure function. Circles and triangles are NMC and ZEUS fits, respectively, at $Q^2 = 70$ GeV^2. The line symbol is the CTEQ6M fit. The lines are the results of our model Set 3g (spin-0 and spin-1 diquark), Set 1g (only spin-0 diquark), Set 2g (no diquark), and Set 3.

TABLE III. GSR results for this work, NMC [26], ZEUS [27,28], and CTEQ6M five-flavor [29] at $Q^2 = 70\ \mathrm{GeV}^2$.

	Set 3g	Set 2g	Set 1g	NMC	ZEUS	CTEQ6M-5f
GSR	0.265	0.266	0.277	0.212	0.232	0.236

reasonably well with the NMC and ZEUS results for nucleon F_2 structure functions, down to x about 0.02, for the cases for which we had introduced gluons in the core nucleon. Our calculation also showed that the meson cloud model is a source of sea-quark asymmetry and Gottfried sum-rule violation. However, our GSR violation was not as pronounced as observation. One could improve on this by including the vector mesons in the model. However, to get the whole picture one needs to take into account other sources, such as the Pauli effect, that could contribute to the violation.

APPENDIX

Following the work done by Barone and collaborators [21], one can consider a transition $v(x) \to q(x) + g(x)$, where $v(x)$ is the initial valence quark distribution in the quark model and $g(x)$ is the gluon distribution generated in the process. Knowing $v(x)$, one can calculate $q(x)$ and $g(x)$ in the following way:

$$q\left(x, Q_1^2\right) = v(x)\left[1 - \int_0^1 dy G\left(1-y, Q_1^2, 0\right)\right] + \int_x^1 \frac{dy}{y} G\left(1-y, Q_1^2, 0\right) \times \left[v\left(\frac{x}{y}\right) - yv(x)\right], \tag{A1}$$

$$\tilde{g}\left(x, Q_1^2, 0\right) = \int_x^1 \frac{dy}{y} v\left(\frac{x}{y}\right) G\left(y, Q_1^2, 0\right), \tag{A2}$$

where the flux of gluons generated from the target quark is

$$G\left(x, Q_1^2, 0\right) = \frac{4}{3}\int_0^{Q_1^2} d^2\vec{k}\frac{\alpha_s(\vec{k}^2)}{2\pi} V\left(-k_g^2\right) \times \frac{\left([1+(1-x)^2]\vec{k}^2 + x^4 m_f^2\right)}{x\left[\vec{k}^2 + (1-x)\mu_G^2 + x^2 m_f^2\right]^2}, \tag{A3}$$

the gluon's virtuality is

$$-k_G^2 = \frac{\vec{k}^2 + x^2 m_f^2}{(1-x)}, \tag{A4}$$

$V(\vec{k})$, the vertex function related to the charge form factor of the nucleon, is

$$V(\vec{k}) = 1 - F_{\mathrm{charge}}(3\vec{k}^2), \tag{A5}$$

m_f is the mass of the quark with flavor f, and μ_G is the effective mass of gluons, introduced so that the color forces do not propagate beyond the confinement radius, and is taken to be about 145 MeV.

To perform the next step of evolution from Q_1^2 to $Q_2^2 (Q_2^2 > Q_1^2)$, one repeats this procedure by replacing $v(x) \to q(x, Q_1^2)$ and $G(x, Q_1^2, 0) \to G(x, Q_2^2, Q_1^2)$, which leads to new gluon distribution

$$g\left(x, Q_2^2\right) = \tilde{g}\left(x, Q_2^2, Q_1^2\right) + \tilde{g}\left(x, Q_1^2, 0\right), \tag{A6}$$

and obviously these along with Eq. (A1) will lead to $q(x, Q_2^2)$. This procedure can be repeated in small steps until one reaches the desired final Q^2, which in our case is 0.5 GeV^2. At this momentum transfer is where we introduce the meson cloud and evolve the distributions to the final momentum transfer.

[1] F. Zamani, Phys. Rev. C **68**, 055202 (2003).
[2] F. Zamani and D. Saranchak, Phys. Rev. C **63**, 065202 (2001).
[3] F. Zamani, Phys. Rev. C **58**, 3641 (1998).
[4] P. A. M. Dirac, Rev. Mod. Phys. **21**, 392 (1949).
[5] H. Leutwyler and J. Stern, Ann. Phys. (NY) **112**, 94 (1978).
[6] M. G. Fuda, Ann. Phys. (NY) **197**, 265 (1990).
[7] M. G. Fuda, Ann. Phys. (NY) **231**, 1 (1994).
[8] M. Burkardt, Adv. Nucl. Phys. **23**, 1 (1996).
[9] F. Schlumpf, Ph.D. thesis, University of Zurich, 1992.
[10] F. Schlumpf, Phys. Rev. D **47**, 4114 (1993).
[11] V. B. Berestetskii and M. V. Terent'ev, Sov. J. Nucl. Phys. **24**, 547 (1976).
[12] V. B. Berestetskii and M. V. Terent'ev, Sov. J. Nucl. Phys. **25**, 347 (1977).
[13] H. J. Melosh, Phys. Rev. D **9**, 1095 (1974).
[14] Z. Dziembowski, C. J. Martoff, and P. Zyla, Phys. Rev. D **50**, 5613 (1994).
[15] C. M. Shakin and W.-D. Sun, Phys. Rev. C **53**, 3152 (1996).
[16] V. R. Zoller, Z. Phys. C **53**, 443 (1992).
[17] N. N. Nikolaev, A. Szczurek, J. Speth, and V. R. Zoller, Z. Phys. A **349**, 59 (1994).
[18] V. N. Gribov and L. N. Lipatov, Sov. J. Nucl. Phys. **15**, 438 (1972).
[19] G. Altarelli and G. Parisi, Nucl. Phys. **B126**, 298 (1977).
[20] Yu. L. Dokshitzer, Sov. Phys. JETP **46**, 641 (1977).
[21] V. Barone, M. Genovese, N. N. Nikolaev, E. Predazzi, and B. G. Zakharov, Int. J. Mod. Phys. A **8**, 2779 (1993).
[22] H. Holtmann, A. Szczurek, and J. Speth, Nucl. Phys. **A596**, 631 (1996).
[23] B. Holzenkamp, K. Holinde, and J. Speth, Nucl. Phys. **A500**, 485 (1989).
[24] G. E. Brown and W. Weise, Phys. Rep. **22**, 279 (1975).
[25] M. Miyama and S. Kumano, Comput. Phys. Commun. **94**, 185 (1996).

[26] P. Amaudruz *et al*., Phys. Lett. **B295**, 166 (1992).
[27] M. Arneodo *et al*., Phys. Lett. **B364**, 107 (1995).
[28] J. Rautenberg, Ph.D. thesis, University of Bonn, 2004.
[29] S. Chekanov *et al*., Phys. Rev. D **67**, 012007 (2003).
[30] S. Chekanov *et al*., Eur. Phys. J. C **21**, 443 (2001).
[31] J. Pumplin, D. R. Stump, J. Huston, H. L. Lai, P. Nadolsky, and W. K. Tung, J. High Energy Phys. 07 (2002) 012.
[32] K. Gottfried, Phys. Rev. Lett. **18**, 1174 (1967).
[33] P. Amaudruz *et al*., Phys. Rev. Lett. **66**, 2712 (1991).
[34] M. Arneodo *et al*., Phys. Rev. D **50**, R1 (1994).